Technical University of Denmark

DTU

Optimization of Integrated Electro-Absorption Modulated Laser Structures for 100 Gbit/s Ethernet Using Electromagnetic Simulation

Johansen, Tom Keinicke; Kazmierski, Christophe; Jany, Christophe; Jiang, Chenhui; Krozer, Viktor

DTU Library
Technical Information Center of Denmark

Optimization of Integrated Electro-Absorption Modulated Laser Structures for 100 Gbit/s Ethernet Using Electromagnetic Simulation

Tom Johansen*, Christophe Kazmierski†, Christophe Jany†, Chenhui Jiang*, and Viktor Krozer*

*Technical University of Denmark, Oersted-DTU, Section of Electromagnetic Systems,

2800 Kgs. Lyngby, Denmark, Email: tkj@oersted.dtu.dk

†Alcatel-Thales III-V Lab, F-91461 Marcoussis Cedex, France

Abstract— **In this paper three options for very-high bit rate integrated electro-absorption modulated laser (EML) structures are investigated using electromagnetic simulation. A physics based distributed equivalent circuit model taking the slow-wave propagation characteristics of the modulation signal into account is proposed for the electro-absorption modulator (EAM) electrode arrangement. This model makes it possible to apply an EM/circuit co-simulation approach to estimate the electrical to optical transmission bandwidth for the integrated EML. It is shown that a transmission bandwidth of 70 GHz seems feasible with the investigated EML structures if the driving impedance is reduced to 25 Ω. It is also shown that the influence of electromagnetic cross-talk between components can be neglected in the estimation of the transmission bandwidth even in the case of very short separation zones. Finally, a slight decrease in transmission bandwidth is observed for an EML structure without ground pillars.**
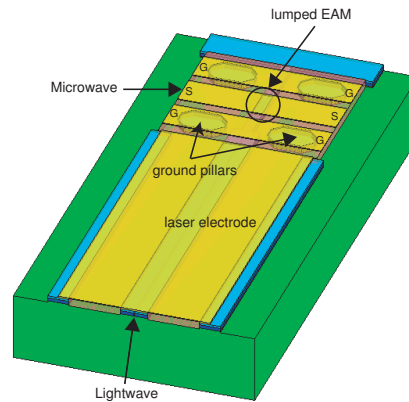
Fig. 1. 3D view of the integrated EML structure (option 1)

I. Introduction

The projected increase in data traffic motivates the development of very high bit rate optoelectronic transceivers suitable for 100 Gbit/s Ethernet type applications. Recently, the European Commission has launched the GIBON project to focus on the technology that will be used in the future for the integration of the highest speed optoelectronic transducers with their driving electronics [1]. Guidelines for the realization of these very-high bit rate integrated devices will be given by supporting electromagnetic (EM) simulation activities.

The electro-absorption modulator (EAM) fabricated on InP is a widely used transmitter component in high bit rate optical communication systems [2]-[3]. For the intended bit-rate of 100 Gbit/s the EAM offers several advantages such as large absorption variations at low driving voltages, very small size, and mature integration with a laser. The electrical to optical transmission bandwidth for an EAM is approximately limited by the time-constant $C_s(Z_o/2 + R_s)$, where Z_o is the driver impedance, C_s the EAM junction capacitance, and R_s the EAM series resistance [4]. To obtain a sufficiently large transmission bandwidth (>70 GHz) driver impedances $< 50\Omega$ are investigated in the GIBON project. The EAM will be monolithic integrated with a laser on InP to form an electro-absorption modulated laser (EML) structure suited for 100 Gbit/s. It is the focus of this paper to describe an EM/circuit simulation approach to investigate the performance of integrated EML structures for 100 Gbit/s Ethernet applications.

II. Integrated EML Structures

A 3D view of the integrated EML structure proposed in the GIBON project is shown in Fig. 1. The length of the EML chip is 710μm including 220μm for the EAM part. To avoid any curves in the RF path an orthogonal microwave and lightwave propagation direction is proposed. A lumped EAM is included in the GSG electrode arrangement. The modulator length has been fixed at 50 μm to give a good compromise between RC-parasitics and extinction ratio. A single active layer containing a p-i-n optical core is used for both the laser and the modulator part. The p-i-n optical core consists of an AlGaInAs multiquantum-well (MQW) stack. Electrical isolation between the two components are achieved using H+ implantation. A heavily doped n-type InP substrate acts like the common ground electrode for the laser and modulator. A BCB polymer embedding the optical core reduces capacitance and provide isolation.

A. GSG design options

In this subsection the three different structures for the integrated EML investigated in this paper will be described.

1) Option 1: This structure is characterized by a 43μm distance between the laser end and beginning of the EAM. Ground pillars provide ground connection to the InP n-type substrate.

2) Option 2: The next structure is identical to the first structure except for a reduced distance between the laser end

Fig. 3. a) A section of EAM electrodes illustrating circuit elements. b) Elements of distributed equivalent circuit model.
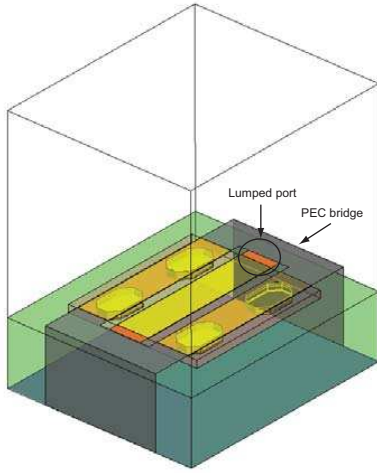
Fig. 2. Ansoft HFSS simulation setup for the EAM electrode arrangement.

and the beginning of the EAM in order to lower the optical loss in the separation zone. Electromagnetic cross-talk is a concern with this structure and should be investigated.

3) Option 3: The final structure is identical to the first structure except the ground pillars are removed. This structure is investigated to check if the ground pillars are really necessary.

III. EAM Electrode Arrangement

The starting point for our investigations has been to develope a distributed equivalent circuit model for the EAM GSG electrode arrangement. The setup in the commercial available simulator, Ansoft HFSS, is shown in Fig. 2. The coplanar excitation of the structure is obtained using lumped ports located across a gap between the signal line and a vertical PEC bridge which connects the two ground conductors together. The PEC bridge is wrapped around the edge to avoid problems with a floating substrate. This excitation resembles very well the measurement situation encountered using GSG probes but may also represent the excitation coming from the driver chip in the case a flip-chip approach. Unfortunately, a parasitic inductance and capacitance are associated with this excitation scheme. These parasitic elements must be evaluated and removed from the EM simulation results to obtain an accurate model of the electrode arrangement. Details in our parasitic removal method applied to EM simulation results can be found in [5]. The simulation structure is surrounded by an air box possessing the radiation boundary condition.

A. EAM Electrode Modeling

The Au electrodes are separated from the heavily doped InP substrate by a thin layer of BCB and thus forms a metal-insulator-semiconductor structure. It is well-known that this transmission line structure supports the slow-wave mode where the electrical field is concentrated in the isolating layer
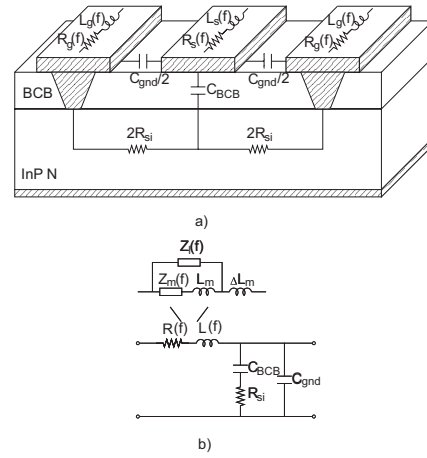
beneath the center conductor while the magnetic field freely penetrates into the substrate [6]. This separation between the electric and magnetic field gives rise to the low-loss slow-wave mode of propagation. EM simulations performed on the EAM electrode arrangement verifies the slow-wave propagation mode even at frequencies up to 110 GHz with an associated low attenuation of $\approx 2dB/mm$.

Fig. 3a) shows a section of the EAM electrodes. The elements of the distributed equivalent circuit model in Fig. 3b) follow from the physical structure in Fig. 3a). An inductance L_m is associated with the longitudinal current which flows on the conductors. Induced Eddy-currents in the substrate are in parallel with this current flow. The effect of the induced Eddy-currents can be represented in the distributed equivalent circuit model as a parallel impedance $Z_l(f)$ calculated as

$$Z_l(f) \approx \alpha(1+j)/(\delta_s \sigma_s W) \qquad (1)$$

where δ_s is the substrate skin depth, f is the frequency, σ_s is the conductivity of the substrate, and W is the width of the center conductor. The above impedance can be deduced from the magnetic vector potential considering a single current sheet of width W located above the substrate. The pre-factor α is a correction factor to take into account the actual geometry of the EAM electrode arrangement. The additional inductance ΔL_m serves the same purpose. To take the metallic conductive losses into account an impedance $Z_m(f)$ is introduced in series with L_m. This impedance is given by

$$Z_m(f) \approx (1+j)/(\delta_m \sigma_m W) \qquad (2)$$

where δ_m and σ_m are the metal skin depth and conductivity of the metal, respectively. The capacitance C_{BCB} and resistance R_{si} are associated with the transverse electric field confined to the dielectric layer underneath the center conductor. There is also a capacitance C_{gnd} associated with the transverse electric field in the air region.
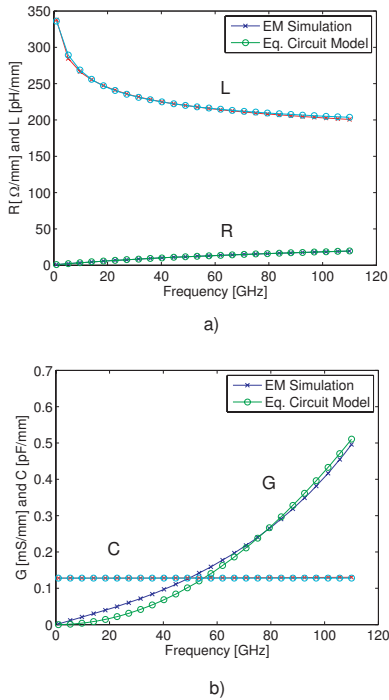
Fig. 4. Comparison of EM simulated and modeled RLGC parameters for EAM electrodes.

In Fig. 4 the per-unit-length RLGC transmission line parameters extracted from the EM simulation results of the EAM electrode arrangement are compared with the developed model in Fig. 3b). It is observed that the developed model very accurately capture the dispersive behaviour of the per-unit-length RLGC parameters up to a frequency of 110 GHz.

IV. EM/CIRCUIT CO-SIMULATION APPROACH

A. Equivalent circuit model for EML structure

To investigate the EML bandwidth potential of the EML structure the equivalent circuit model shown in Fig. 5 is purposed. The model has been implemented into the Agilent ADS microwave circuit simulator allowing both small-signal AC responses and S-parameters to be easily calculated. Distributed transmission line sessions are included at the signal generator and load ends to take the slow-wave mode propagation characteristic of the modulating signal on the electrodes into account. The EAM part can often be modeled using a series resistance R_s and capacitance C_s, and a dynamic photocurrent-resistance R_{ph} [7]. The dynamic photocurrent resistance must be included to predict the effect of the optical power on the electrical-to-optical (E/O) response. The E/O response is determined by the ratio of the voltage over the EAM diode junction V_{out} to the voltage $V_{in}/2$ applied to the EML structure in the case of zero input reflection. A shunt capacitor C_p depending on the i-layer thickness in the region
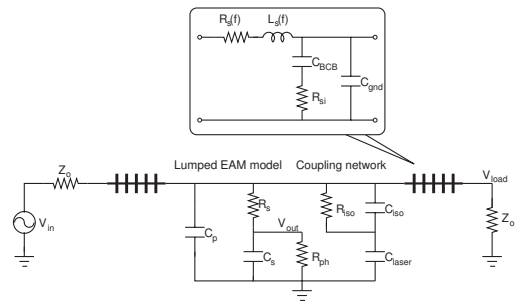

Fig. 5. Equivalent circuit model for EML bandwidth estimation. Insert shows distributed equivalent circuit model for electrode arrangement.

outside the EAM MQW stack is also included. To take the coupling to the laser part into account the isolation resistance R_{iso} and capacitance C_{iso} are used. The laser part itself is modeled here with a single capacitor C_{laser}.

B. EM simulation setup

It should be noticed that the lumped equivalent circuit model for the EAM diode junction depends on the optical power and applied signal swing in a nonlinear manner, and hence can not be predicted by EM simulation. Previously, EM simulation of EAMs has been performed by substitution of the MQW stack in the EAM diode junction with a dielectric material having an averaged permittivity [8]. In this work a slightly different approach is followed in that the lumped equivalent circuits for the MQW stack in the EAM and laser junction parts are included into the Ansoft HFSS EM simulation. This can be accomplished by using lumped RCL-boundary conditions available in the Ansoft HFSS simulator. An expanded view of the details in the EAM region shown in Fig. 6 illustrates the setup in Ansoft HFSS. For the EAM junction typical values for the capacitance C_s and dynamic photocurrent-resistance R_{ph} are substituted, while for the laser MQW a
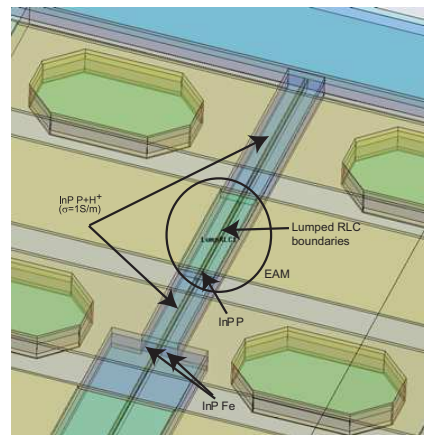

Fig. 6. Expanded view showing EAM region details for Ansoft HFSS integrated EML simulation setup.
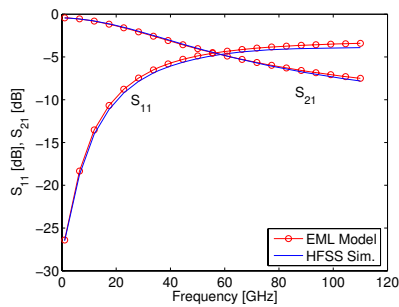
Fig. 7. Comparison of EM simulated and modeled electrical reflection and transmission responses for the EML structure (option 1).

Fig. 8. Electrical to optical transmission characteristics for EML structures. The driver impedance level is reduced to $Z_o = 25\Omega$.

single capacitor C_{laser} is substituted. The junction capacitance values can be determined experimentally from low-frequency C-V measurements, while the photocurrent resistance can be either calculated or measured with an optical input power to the EAM. In this way it is possible to obtain a more realistic view of the optical and electrical properties of the full EML structure from the EM simulation. The EM simulation results contain all the electromagnetic information of the EML structure, such as the electrical-to-electrical (E/E) transmission, port reflections, and coupling to the laser part. The output voltage V_{out} across the EAM junction, however, which determines the E/O response is not readily available from the EM simulation result. Therefore our approach is to fit the remaining elements (R_s, C_p, C_{iso}, and R_{iso}) of the equivalent circuit model in Fig. 5 to the EM simulation results. An AC simulation can then be used to determined the E/O transmission bandwidth including the effect of driver impedances $Z_o < 50\Omega$.

The equivalent circuit modeling approach is verified in Fig. 7 by comparison of the EM simulated and modeled electrical reflection and transmission responses for the EML structure. It should be mentioned that the cross-coupling network has a very small influence on the simulated response. Especially it is difficult to extract a reliable value of the isolation resistance R_{iso} from the EM simulation result. To obtain a better estimate this resistance is calculated based on geometrical details.

V. EML BANDWIDTH ESTIMATIONS

In this section the E/O transmission bandwidth for the three different structures for the integrated EML (option 1-3) described in section II is investigated. In order to investigate potential problems with electromagnetic cross-talk, option 2, with reduced separation distance between the laser end and the beginning of the EAM is simulated in Ansoft HFSS. The obtained EM simulation result can not be distinguished from those of option 1. The reason for this is that even with the shorter separation zone the calculated isolation resistance will still be on the order of hundreds of kilo-ohms due to the H+ implantation. The electromagnetic cross-talk between components can therefore be neglected in the estimation of the transmission bandwidth as clearly observed in Fig. 8.
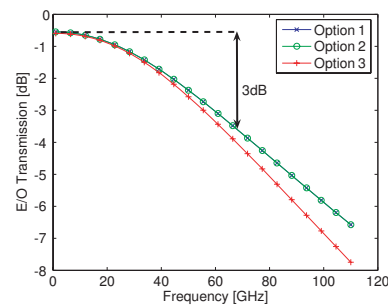
Notice that an E/O transmission bandwidth of nearly 70 GHz is obtained when the driver impedance level is reduced to $Z_o = 25\Omega$. Even larger bandwidths are possible with further reduction of the driver impedance. To investigate if the ground pillars are really necessary, option 3, with ground pillars removed is simulated in Ansoft HFSS. The explanation of the slightly lower E/O transmission bandwidth observed in Fig. 8 is as follows. Without proper connection of the ground conductors to the heavily doped InP substrate a microstrip-like mode is allowed to propagate along the GSG electrode. As a consequence the propagation characteristics of the GSG electrode changes and less of the supplied electromagnetic energy reaches the EAM diode junction. Instead of repeating the distributed equivalent circuit modeling for the GSG electrode without ground pillars the EAM part is substituted with an additional lumped port in the Ansoft HFSS setup. The lumped EAM model previously determined for the EML structure, option 1, is attached to this additional port in the Agilent ADS simulation.

VI. CONCLUSION

In this paper three different EML structures for 100 Gbit/s have been investigated using EM simulation. Development of a distributed equivalent circuit model for the GSG electrode arrangement makes an EM/circuit simulation approach for determining the E/O transmission response possible. Employing a reduced driver impedance of 25Ω in connection with the integrated EML structures estimates an E/O transmission bandwidth of nearly 70 GHz. The influence of electromagnetic cross-talk on the bandwidth was shown to be negligible even in the case of very short separation zones. The transmission bandwidth for EML structure without ground pillars demonstrate slightly lower bandwidth than the two other structures investigated. Measurements performed on EML chips should be available at the time of the conference.

REFERENCES

[1] The GIBON website. [Online]. Available: http://www.ist-gibon.eu/index.htm

[2] M. L. Pallec *et al.*, "42 GHz bandwidth InGaAlAs/InP electro absorption modulator with a sub-volt modulation drive capability in a 50 nm spectral range," in *Proc. IPRM 04*, 2004.

[3] H. Fukano *et al.*, "Very-low-driving-voltage electroabsorption modulators operating at 40 Gb/s," *J. Lightwave Technol.*, vol. 24, no. 5, pp. 2219–2224, 2006.

[4] H. Arimoto *et al.*, "A 40-Gbit/s electro-absorption modulator with a record modulation efficiency (50 GHz/V) enhanced by a novel technique hybrid integration on the driver IC," in *Proc. LEOS 03*, 2003, pp. 646–647.

[5] T. K. Johansen *et al.*, "Em simulation accuracy enhancement for broadband modeling of on-wafer passive components," in *To be published Proc. EuMIC 07*, 2007.

[6] Y. R. Kwon *et al.*, "Quasi-TEM analysis of slow-wave mode propagation on coplanar microstructure MIS transmission lines," *IEEE Trans. Microwave Theory Tech.*, vol. MTT-35, no. 6, pp. 545–551, 1987.

[7] G. L. Li *et al.*, "Concise RF equivalent circuit model for electroabsorption modulators," *Electron. Lett.*, vol. 36, no. 9, pp. 818–820, 2000.

[8] T. Yamanaka *et al.*, "Lightwave-microwave unified analysis of electroabsorption modulators integrated with RF coplanar waveguides," *IEEE Photon. Technol. Lett.*, vol. 17, no. 12, pp. 2562–2564, 2005.